Morphological and Rheological Properties of (Low-Density Polyethylene)/Thermoplastic Starch Blend: Investigation of the Role of High Elastic Network

Saeed Mortazavi, Ismail Ghasemi, Abdulrasoul Oromiehie
Plastic Department, Iran Polymer and Petrochemical Institute, Tehran, Iran

Rheological and morphological properties of low-density polyethylene (LDPE) and thermoplastic starch (TPS) with low-density polyethylene-*grafted*-maleic anhydride as a compatibilizer were investigated. The results showed that the circularity of the droplets decreased with increasing TPS content. The presence of compatibilizer led to finer morphology and higher continuity. The rheological analyses showed that TPS and compatibilizer can increase elasticity and viscosity of the blend dramatically. In addition, the compatibilizer enhanced the compatibility of the blends, as evidenced by the shifting of the relaxation time peak of TPS to longer times. The rheological properties of the neat components and their blends were discussed by the Carreau-Yasuda and fractional Zener models. The fractional Zener model results proved the existence of network structure in the compatibilized blends. The transient properties of blends showed that TPS and compatibilized blends had strong overshoot compared with the uncompatibilized blend, owing to the formation of high elastic network in their structure. J. VINYL ADDIT. TECHNOL., 00:000–000, 2014. © 2014 Society of Plastics Engineers

INTRODUCTION

Disposal of large amounts of synthetic polymers in the environment has caused much environmental pollution and increased interest in the nontoxic and biodegradable polymers from nature, such as starch. Starch is a natural, renewable, and inexpensive polymer, which is biodegradable in environments. In order to process starch with conventional plastic equipment, gelatinization should be done to produce thermoplastic starch (TPS). In this method, the structure of starch granules destructs under shear and high-temperature conditions with plasticizers, such as water and glycerol [1]. However, TPS is very moisture-sensitive with poor mechanical properties [2].

These drawbacks can be improved by blending starch with other polymers, such as polyolefins. Because polyethylene is one of the most consumed non-biodegradable polymers and is used extensively in packaging and agricultural films, many attempts have been made on the binary blend of polyethylene/starch to enhance the biodegradability of the polyethylene [3–8].

Because of the mismatch of hydrophobicity of these polymers, many copolymers, such as poly(ethylene-*co*-acrylic acid), poly(ethylene-*co*-vinyl alcohol), poly(ethylene-*co*-glycidyl methacrylate), (methyl methacrylate)-butadiene-styrene copolymer, and poly(ethylene-*grafted*-maleic anhydride) (PE-*g*-MA), as compatibilizers for blends have been reported in the literature [9–19]. However, the latter is the most common because the maleic anhydride groups of PE-*g*-MA can react with the hydroxyl groups of starch, while the PE chains interact with the PE matrix [20, 21]. As a result, the interfacial tension between two phases decreases and the particle sizes are significantly lower compared with the uncompatibilized blend [22, 23].

As the compatibilization process occurs in the melt state, the rheological properties of the blends can be affected greatly and must be studied. Although many studies were performed on the effect of the compatibilizer on the morphology and mechanical properties of polymer blends, there was less attention on the effect of compatibilization on their rheological properties. In addition, most of these studies were done in an oscillatory situation and under a small amplitude of deformation with opposing results reported. For example, the addition of a block copolymer to polystyrene (PS)/(polymethyl methacrylate) blends leads to an increase in viscosity [24]. The same results were obtained for compatibilized polyamide blends with polyamide (PA)/polypropylene (PP) [25]. However, the PA/PS blend showed that compatibilization led to a decrement in the blend's viscosity at high shear rates [26]. On the other hand, the addition of styrene-butadiene-styrene block copolymer showed no effect on the morphological and rheological properties of polyethylene/styrene (PE/PS) blend [27]. Velankar et al. found that the addition of the compatibilizer slightly increased the terminal complex viscosity of polydimethylsiloxane/polyisobutylene blend at all ratios of viscosity [28]. Sailer and Handge showed that during reactive mixing of PA6/styrene acrylonitrile compatibilized blend, an elastic network

---

Correspondence to: Ismail Ghasemi; e-mail: I.ghasemi@ippi.ac.ir

DOI 10.1002/vnl.21360

formed between the PA6 domains [29]. Entezam et al. used the fractional Zener model (FZM) to prove the existence of the network-like structure in compatibilized (polyethylene terephthalate)/PP blend [30]. In the case of PE/TPS blends, very few studies have been conducted on its rheological properties. Ning et al. studied the blend of TPS and linear low-density polyethylene and found that this blend showed shear thinning behavior [31, 32].

In this study, the morphological and rheological properties of low-density polyethylene (LDPE)/TPS/(low-density polyethylene-*grafted*-maleic anhydride) (LDPE-*g*-MA) with different compositions were investigated in detail. The rheological experiments were accomplished in frequency sweep and transient modes. The obtained experimental data were compared with well-known rheological models to achieve more knowledge about the structure of this blend.

EXPERIMENTAL

Materials

Commercial LDPE resin, LDPE0200 (melt flow index = 2 g/10 min, density = 0.92 g/cm^3) was prepared from Bandar Imam Petrochemical Co. (Iran). Wheat starch was obtained from Glucosan Co. (Tehran, Iran), which consisted of 25 wt% amylose and 75 wt% amylopectin, with a moisture content of less than 10 wt% (as measured by analysis by thermogravimetry). Analytical-grade glycerol was purchased from Dr. Mujalli Co. (Tehran, Iran). LDPE-*g*-MA with 1.5 wt% grafted maleic anhydride with a melt flow index of 2 g/10 min was provided by Grankin Co. (Tehran, Iran) and used as compatibilizer.

Sample Preparation

Starch, LDPE, and LDPE-*g*-MA were dried in an oven at 60°C for 24 h. TPS was prepared by gelatinization of starch granules with 36 wt% of glycerol in a Haake plastograph internal mixer (HBI System 90) at 130°C for 2 min with a rotor speed of 60 rpm. The prepared TPS was then blended with LDPE and LDPE-*g*-MA in the Haake mixer at 130°C for 5 min with a rotor speed of 80 rpm. The blend compositions are depicted in Table 1. The samples for rheological and morphological tests were prepared via a compression-molding process (Toyosiki Press, Tokyo, Japan) at a temperature of 160°C and a pressure of 25 MPa. For morphological analysis, the samples were rectangular bars of with a thickness of 1 mm, and for rheological tests, cylindrical pieces with a diameter of 25 mm and a thickness of 2 mm were prepared.

TABLE 1. Component composition of the samples.

Sample code	LDPE (wt%)	TPS (wt%)	TPS (vol%)[a]	LDPE-*g*-MA
LDPE	100	0	0	0
TPS	0	100	100	0
LTC20	75	20	15	5
LTC35	60	35	27	5
LTC60	35	60	51	5
LTC75	20	75	68	5
LTU60	40	60	51	0

[a] The density of TPS was assumed to be 1.31 g/cm^3 to calculate its volume composition [33].

Morphological Analysis

Before testing, the samples were cryogenically fractured in liquid nitrogen. The samples were then etched at room temperature with 6N HCl solution for 12 h to extract the TPS phase. The etched samples were washed with water and dried in an oven for 24 h. The morphologies of the blends were investigated by scanning electron microscopy (SEM) by using a Vega Tescan model microscope. The samples were coated with gold before the test. The size of the particles was analyzed by using ImageJ software. For each sample, at least 200 particles were considered to characterize their morphological parameters.

Rheological Analysis

All the rheological tests were carried out by using an Anton Paar Physica shear rheometer, MCR 300 (Graz, Austria). Parallel plate geometry was used with a plate diameter of 25 mm. The gap between the plates was set to 1 mm. Strain sweep tests were performed at a constant frequency of 1 rad/s to ensure that the dynamic tests were done in the linear viscoelastic region. The shear strain amplitude was set to 0.3% for frequency sweep tests. The angular frequency range was from 0.02 to 600 rad/s. All the measurements were performed at 130°C. The start-up shear flow tests were performed at 130°C; the shear rate was set at 0.2 s^{-1}, and the gap between the plates was 1.2 mm.

RESULTS AND DISCUSSION

Blend Morphology

The SEM micrographs and the particle diameter distributions of the blends are displayed in Figs. 1 and 2. Because the particles have irregular shapes, it is necessary to quantify the particle diameter (d) by using the area of each particle (A):

$$d=\left(\frac{4A}{\pi}\right)^{1/2} \tag{1}$$

As can be seen in Fig. 1, LDPE/TPS blends exhibit droplet-matrix morphology (when the TPS content is 20, 35, and 60 wt%), where LDPE is the matrix. However, at higher concentrations of TPS (75 wt%), co-continuous morphology forms. Similar results were reported for PCL/TPS, which did not form co-continuous structure even at 60 wt% of TPS [33].

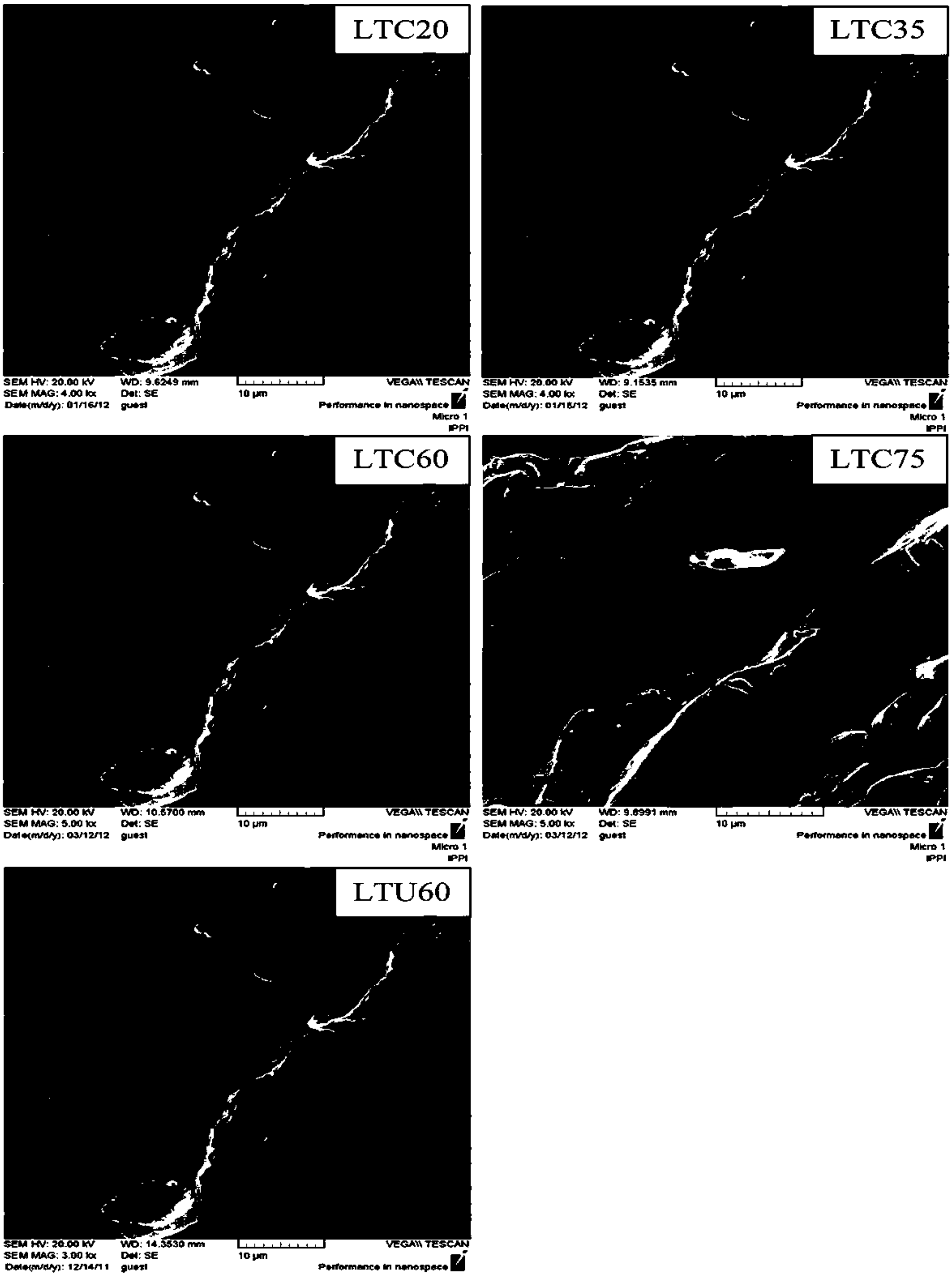

FIG. 1. SEM images of the blends: (a) LTC20, (b) LTC35, (c) LTC60, (d) LTU60.

The histograms showed some large droplets existed in the compatibilized samples, but most of the particles of the compatibilized samples were very small, less than 1.5 μm. Table 2 shows the number-average diameter of the samples. The diameter of compatibilized blend (LTC60) is about half of uncompatibilized blend (LTU60). It is well-known that compatibilizer can reduce the interfacial tension between immiscible phases and hence significantly decrease the size of the dispersed phase [22, 23]. This decrement is in consequence of the esterification between the carboxyl groups of starch, the maleic anhydride groups of LDPE-*g*-MA, and the in situ formation of copolymers at the interface [20, 21]. However, the high elasticity of TPS prevents its droplets from breaking and forming smaller droplets. It is well-known that the high elastic properties led to a lower capillary number than a

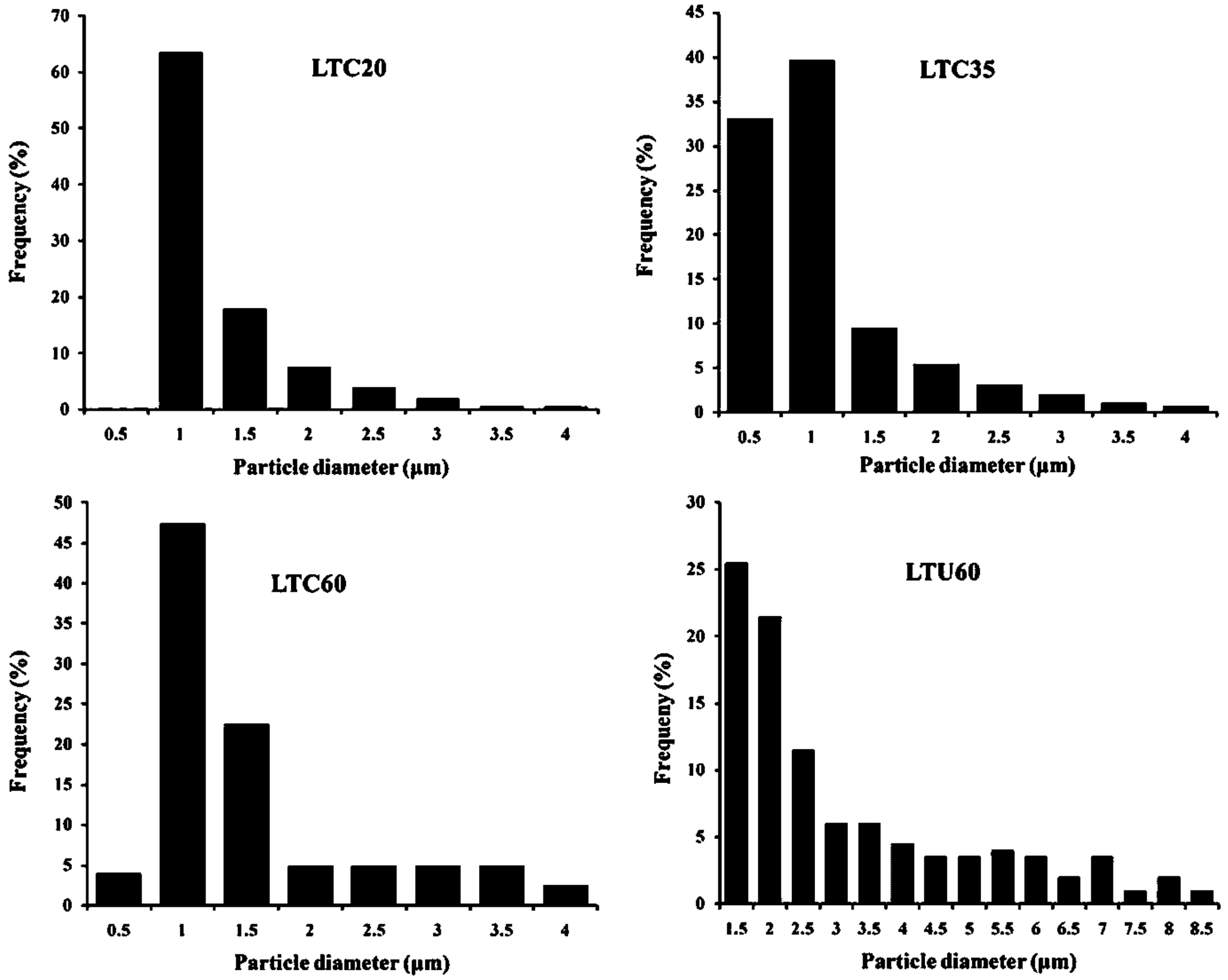

FIG. 2. The distribution of the particle diameter of the LDPE/TPS blends with different compositions.

critical number (Ca_{cr}); therefore, the droplet has a more stable shape and does not break easily [34].

It is expected that, when the concentration of the dispersed phase increases, the particles' diameters become larger through particle-particle coalescence [35]. However, in the compatibilized LDPE/TPS, the particle size diameter does not change significantly with an increase in the weight fraction of the TPS phase from 20 to 60 wt%. In situ compatibilization eliminates coalescence at the higher dispersed phase concentrations and thus the particle diameter does not change significantly with increasing the concentration of the minor phase [36, 37].

The morphology of the blends can also be evaluated by using the concept of "circularity ratio" [38]. This quantity is defined as follows:

$$\text{circularity ratio} = C = 4\pi \frac{A}{(\text{perimeter})^2} \qquad (2)$$

A circularity ratio of 1 means a true circular shape, which indicates droplet-matrix morphology and $C = 0$ describes an infinite long and narrow shape, which implies a high degree of continuity [39].

The circularity ratios of the samples are shown in Table 2. The circularities of compatibilized samples decrease monotonically with an increase in the TPS weight fraction in the blend. However, this decrement is not significant up to 75 wt%, which shows co-continuous morphology. Steinmann et al. reported that in the case of PS/(polymethyl methacrylate) (50/50 wt%), the value of

TABLE 2. The morphology characteristics of the blends.

Formulation code	D_n (± SD[a]) (μm)	Perimeter (± SD) (μm)	Circularity ratio (± SD)
LTU60	3.12 (±2.01)	15.44 (±22.97)	0.65 (±0.26)
LTC20	1.21 (±1.32)	6.29 (±7.51)	0.71 (±0.21)
LTC35	1.23 (±1.50)	5.35 (±9.45)	0.61 (±0.31)
LTC60	1.48 (±1.35)	8.50 (±10.83)	0.54 (±0.30)
LTC75	–	70.14 (±123.56)	0.30 (±0.11)

[a] Standard deviation.

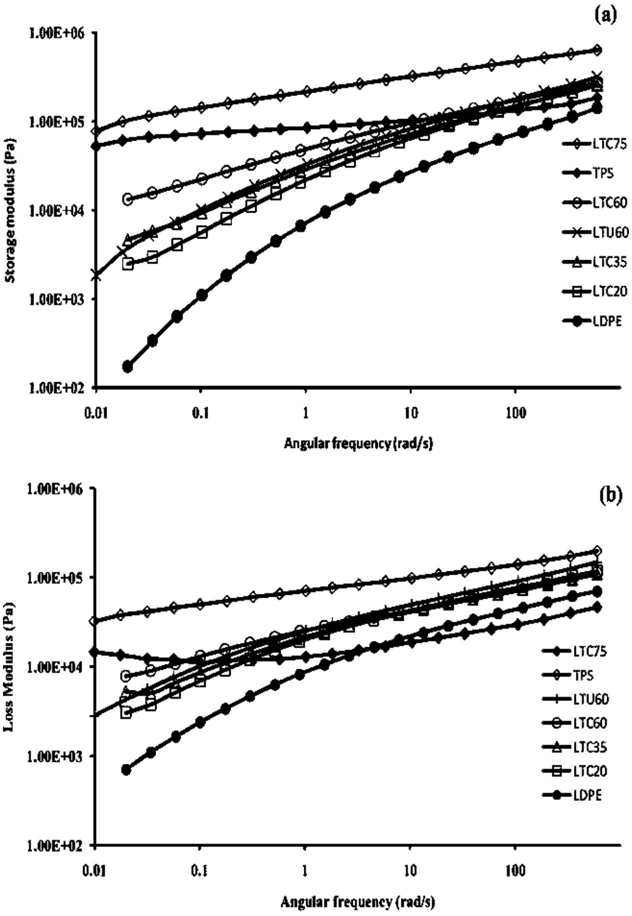

FIG. 3. The storage (a) and loss modulus (b) of LDPE and TPS and their blends.

circularity ratio is about 0.4, and related this low value to a maximum of co-continuity and the phase inversion concentration of the blend [38]. Therefore, it can be concluded that the co-continuous morphology of LTC75 and its low circularity ratio is related to the phase inversion point of the LDPE/TPS blend. This is discussed in more detail later in this paper.

Table 2 also shows that the circularity ratio of the compatibilized blend (LTC60) is somewhat lower than uncompatibilized blend (LTU60). DeLeo et al. showed that the compatibilizers can decrease the circularity when a cluster of droplets forms [40]. Therefore, it can be concluded that a decrease in the circularity ratio is caused by the formation of an elastic network during reactive blending.

Rheological Properties of the Blends

Figure 3 shows the storage (G') and loss modulus (G'') of the blends and pure components. As mentioned previously, the elasticity of the TPS is very high, which is related to its elastic structure. This structure originates from the development of a crystalline elastic network, which is formed by the complex of amylose molecules with lipid molecules and the physical entanglement of starch macromolecules induced by its very high molecular weight [41–43].

It seems that the storage modulus of TPS is larger than the loss modulus over the whole frequency range, which is a common behavior in the gel-like materials. The frequency dependence of elastic and loss modulus of gel materials follows this relation [44]:

$$G'(\omega)=\frac{G''(\omega)}{\tan(n\pi/2)}=\Gamma(1-n)\cos\left(\frac{n\pi}{2}\right)S\omega^{n} \qquad (3)$$

where Γ is the gamma function, S is strength of the gel, and n is the power law index. The best-fit values of S and n for neat TPS were 80,948 and 0.1033, respectively. It is found that when $n>0.5$, $G'<G''$, and oppositely for $n<0.5$. The value of exponent n is reported in the range of 0.19-0.92 for chemically crosslinking gels [44], while for the physical gels, it is much lower [45]. In addition, when the molecular weight exceeds the entanglement threshold, the exponent decreases to much smaller values [46].

In contrast to TPS, the storage modulus of the other samples strongly depends on the angular frequency and increase of TPS content. The most interesting result belongs to LTC75, which has co-continuous structure. The elastic modulus of this sample is not only larger than other blends, but also is a little higher than that of TPS. The results of DeLeo et al. showed that the storage modulus of PI/polydimethylsiloxane reactivity blend was much larger than that of their neat components [47]. The frequency dependence of complex viscosity is shown in Fig. 4. It seems that the viscosity of the blend rises as the TPS content in the blends increases. Bélard et al. used the logarithm additive mixing rule to predict the theoretical value of the blend viscosity (η_b) and evaluate compatibility in starch/PCL blend [48]:

$$\log(\eta_b)-\phi_1\log(\eta_1)+\phi_2\log(\eta_2) \qquad (4)$$

where η_i and Φ_i denote the viscosity and volume fraction of the phase i, respectively. We used this model to study

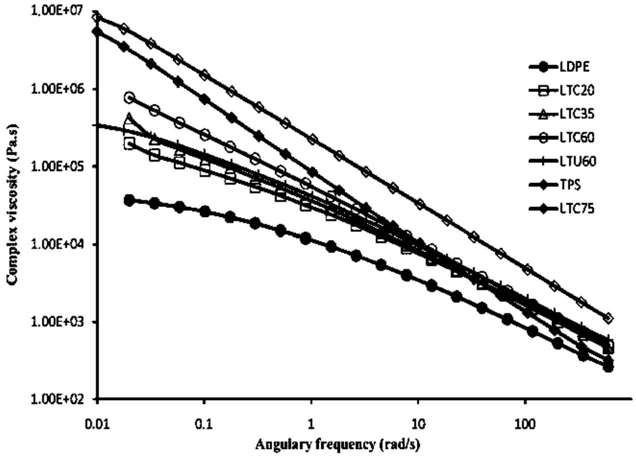

FIG. 4. The complex viscosity of the LDPE, TPS, and their blends.

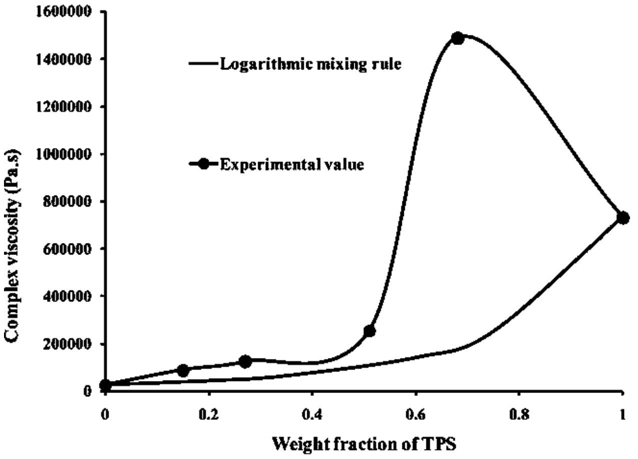

FIG. 5. Positive deviation of complex viscosities of the compatibilized blends from the logarithmic mixing rule (*Eq. 4*). The angular frequency is 0.1 rad/s.

the deviation from experimental data; the results are shown in Fig. 5. As can be seen, there is a large positive deviation from the theoretical viscosity, which confirms good compatibility [49] and implies the existence of an elastic network structure. DeLeo et al. showed that reactive blending enhanced the complex viscosity, especially at low frequency, and related this behavior to the drop clustering [47].

On the other hand, in the uncompatibilized blend, the interface is very weak and therefore the interlayer slip can occur, which causes considerable reduction of the viscosity [50–53].

The rheological data can be used to predict the phase inversion point of the blend. The simplest model for predicting the phase inversion point was proposed by Paul and Barlow [54]:

$$\frac{\phi_1}{\phi_2}=\frac{\eta_1}{\eta_2} \tag{5}$$

In this equation, it is necessary to use a viscosity that is related to the shear rate at the processing condition. The average shear rate ($\dot{\gamma}$) in the internal mixer can be calculated as follows:

$$\dot{\gamma}=\frac{\pi DN}{\delta} \tag{6}$$

where D is the rotor diameter (38 mm), N is the rotor speed (1.33 round per second), and δ (5 mm) is the minimum gap between the rotor and internal wall of mixer. Regarding the dimension characteristics of the internal mixer and the processing condition, the average shear rate was obtained at about 32 s^{-1}. Figure 4 shows that at this frequency the complex viscosity ratio of TPS to LDPE is about 2. Therefore, *Eq. 6* predicts that the phase inversion composition of this blend is 66.6 vol% (75 wt%) of TPS, which is in good agreement with the morphological results. Li and Favis reported similar results for the PCL/TPS blend and found that the phase inversion point was located between 55 and 67 vol% of TPS for this blend [33].

Figure 6 shows tan δ (G''/G') for all the blends and pure components. As already stated, the storage modulus of the TPS is much higher than its loss modulus and thus its damping factor is very low over the entire frequency range. On the other hand, the damping factor for LDPE is larger than 1 for low frequencies. The blends' damping factor decreases with increasing TPS content and the behavior of the blends changes to an elastic state. In addition, the tan δ for compatibilized blend (LTC60) is much lower than the uncompatibilized blend (LTU60). It seems the compatibilizer decreases the damping factor by forming the high elastic network.

Relaxation Spectrum

Relaxation time spectrum can provide useful information about the compatibility of polymer blends [55]. Elastic (G') and loss modulus (G''), which are obtained from rheological data, can be used to calculate the relaxation time spectra. The relations between relaxation spectrum, $H(\lambda)$, and G' and G'' are as follows [56]:

$$G'(\omega)=\int_{-\infty}^{+\infty} H(\lambda)\frac{\omega^2\lambda^2}{1+\omega^2\lambda^2}\mathrm{d}\ ln\,\lambda \tag{7}$$

$$G''(\omega)=\int_{-\infty}^{+\infty} H(\lambda)\frac{\omega\lambda^2}{1+\omega^2\lambda^2}\mathrm{d}\ ln\,\lambda \tag{8}$$

where λ is the relaxation time and ω is the angular frequency.

Many methods exist for the calculation of the relaxation spectrum from rheological data [57]. In this study, the relaxation spectrum was obtained by a nonlinear calculation method [53] by using MCR-300 rheometer software. Figure 7 shows the relaxation time spectra [$H(\lambda)$] of the blends and their neat components. The relaxation spectra of the blends are broad like their components and have two peaks for compatibilized blends, which are related to the relaxation of LDPE and TPS components.

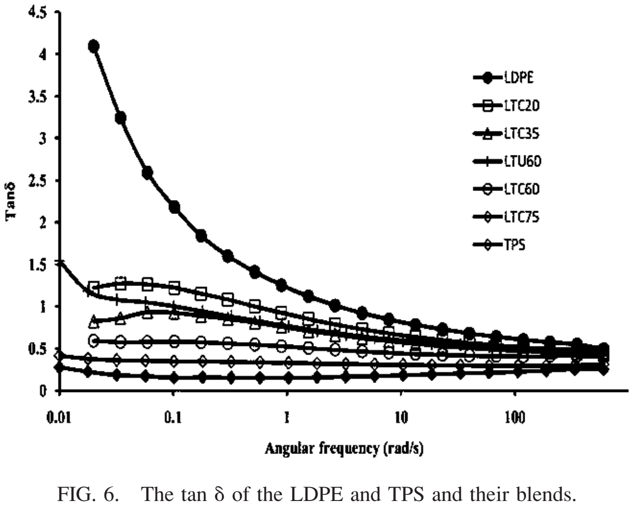

FIG. 6. The tan δ of the LDPE and TPS and their blends.

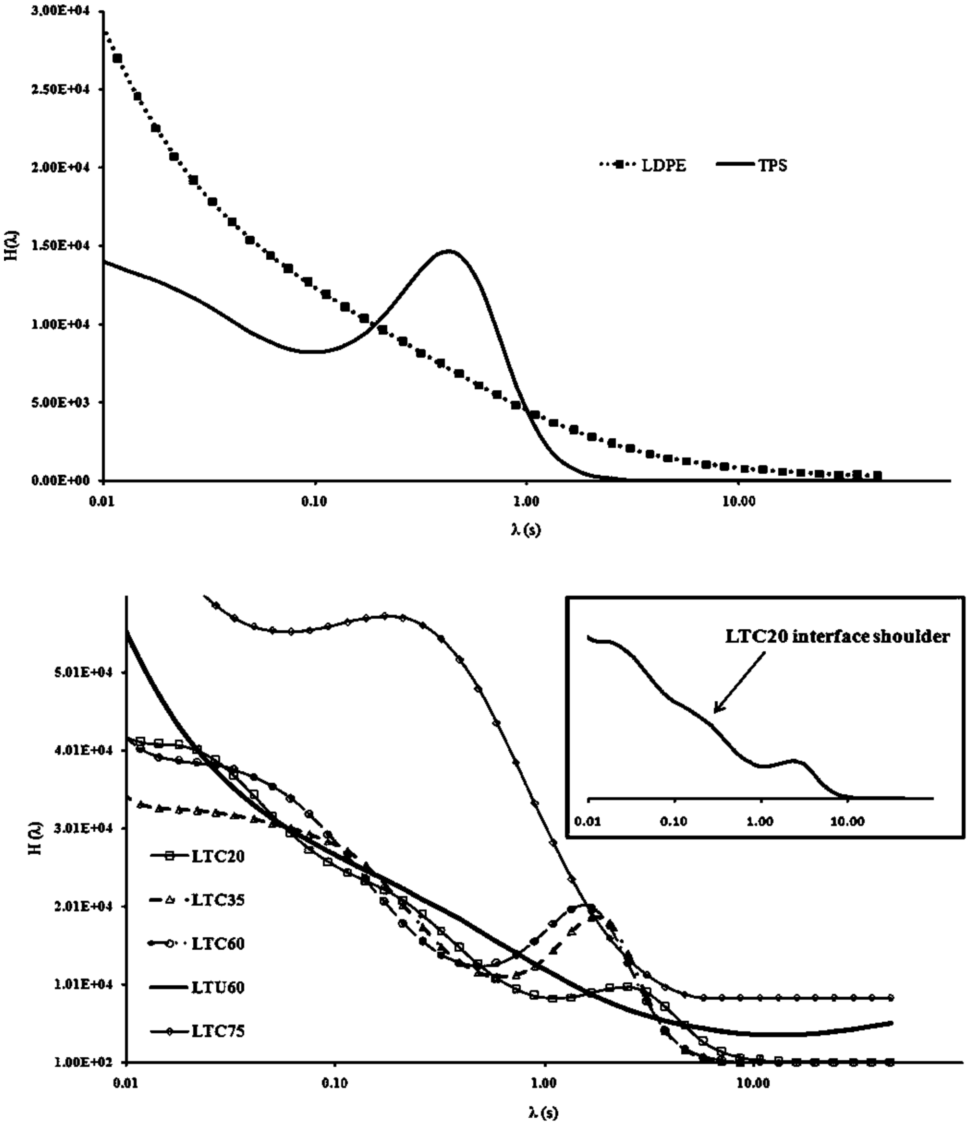

FIG. 7. The relaxation spectra of (a) LDPE and TPS, and (b) their blends.

In the case of compatibilized blends, the characteristic TPS peak moves toward longer times than that of pure TPS. This shift implies an increment of the compatibility between dispersed and matrix phases [58]. Entezam et al. showed that the relaxation peak shifted to longer times for compatibilized PP/(polyethylene terephthalate) blends than the uncompatibilized blend [30].

For the compatibilized blends (especially LTC20), there is a shoulder that is related to interfacial properties. An additional relaxation process was also observed for the compatibilized PE/PA6 blend [59] and was ascribed to the anisotropic interfacial tension on the surface of the drops [60] and also to shape the relaxation of the droplets [56].

Rheological Parameters

The Carreau-Yasuda model is an appropriate model that can fit experimental data of the viscosity of pure polymers and their blends to a wide range of shear rates. Some important parameters such as zero shear viscosity and power law exponent can be obtained from this model. If the Cox-Merz rule is applied for all the samples, this model can be used for dynamic measurements [61–63]:

$$\frac{\eta-\eta_\infty}{\eta_0-\eta_\infty}=[1+(\lambda x)^a]^{\left(\frac{n-1}{a}\right)} \tag{9}$$

where x is shear rate or angular frequency, η_0 is the zero-shear-rate viscosity, η_∞ is the infinite-shear-rate viscosity, λ is a time constant, n is the power law exponent, and a is a dimensionless parameter. These parameters were determined by fitting the model with the experimental data for all formulations and are summarized in Table 3. Regarding this table, the TPS has a very low power law index (n) and shear thinning behavior with slope of about -1. Shear thinning behavior of TPS has been reported frequently [64]. On the other hand, the power law index

TABLE 3. The fitted parameters for Carreau-Yasuda model.

Sample code	η_0 (Pa.s)	N	a	λ (s)	η_∞ (Pa.s)
LDPE	57,635	0.30	0.43	3.39	11.39
TPS	5,015,300	0.07	8.11	75.09	84.81
LTC20	318,830	0.33	0.55	81.24	24.78
LTC35	525,790	0.36	8.11	79.44	41.05
LTC60	1,314,500	0. 27	1.14	78.56	52.23
LTU60	908,170	0.28	0.41	46.18	12.12
LTC75	8,412,100	0.27	5.73	77.54	83.91

for all the blends is approximate to that of pure LDPE. Lacroix et al. indicated that the rheological properties of the blend were governed by matrix, especially at high frequency [56].

In contrast, the zero shear viscosity of the blends is strongly dependent on the TPS content and increases with increasing TPS content in the blend, owing to its high zero shear viscosity. The η_0 of the blend without the compatibilizer (LTU60) is about five times smaller than that of the uncompatibilized blend (LTC60). The compatibilizer effects are evident at low frequencies and therefore zero shear viscosity is strongly changed. Compatibilizer increases interactions not only between the two phases but also between the dispersed phase droplets [49] and forms a network that promotes the zero shear viscosity.

Fractional Zener Model

To describe the complex modulus of the blends, the most common model is the Palierne model. This model relates the viscoelastic properties of the blend with their morphological and the rheological properties of its pure components [65]. However, the rheological properties of the compatibilized blends or the blends with co-continuous morphology cannot predict well with this model [66, 67]. Therefore, for describing the rheological behavior of the samples, the FZM was considered. This model includes two fractional elements in a series that connect with a spring in a parallel mode, as displayed in Fig. 8. It can describe the rheological behavior of the polymer blends and pure components even with solid-like behavior [29]:

$$\begin{gathered}\sigma_{xy}+\tau_0^{\alpha}\frac{d^\alpha}{dt^\alpha}\sigma_{xy}=G_e\left(\gamma+\tau_0^{\alpha}\frac{d^\alpha}{dt^\alpha}\gamma\right)+G_0\tau_0^{\beta}\frac{d^\beta}{dt^\beta}\gamma\\ \alpha=\beta_1-\beta_2>0\\ \beta=\beta_1\end{gathered}\qquad(10)$$

where β_i, τ_0, G_0, and G_e are the fractional exponents, characteristic time, modulus of the fractional parts, and the elastic modulus of the spring, respectively. When $\beta=0$, the rheological behavior of fractional elements is purely linear elastic and, when $\beta=1$, it has purely viscous properties. According to this constitutive equation, the complex modulus is [68]:

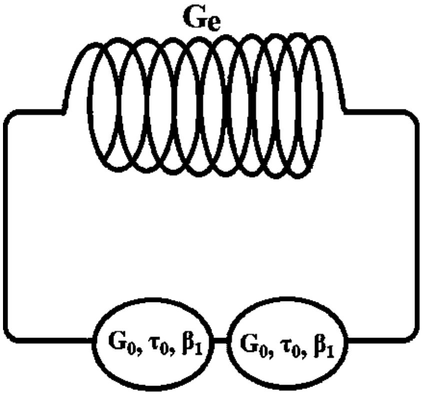

FIG. 8. FZM with elastic spring and fractional elements.

$$G^*(\omega)=G_e+G_0\left(\frac{(i\omega\tau_0)^\beta}{1+(i\omega\tau_0)^\alpha}\right)\qquad(11)$$

Table 4 depicts these parameters, which were obtained from fitting the experimental data to this model. As can be seen, the compatibilized blends have large G_e. The large value of G_e implies the existence of the network structure, which can be attributed to interconnectivity between particles [29]. The uncompatibilized blend has zero value for G_e, which indicates that there is no interaction between TPS particles.

The TPS low β parameter in Table 4 confirms that the rheological properties are related to a solid or very elastic material, as discussed previously. However, this parameter is very close to unity for pure LDPE, which means that this material shows viscose properties. For compatibilized blends, the β parameters are more or less close to that of LDPE even at 60 wt% TPS, which means that the frequency dependency of rheological properties of the blends is mostly controlled by the matrix (LDPE), as mentioned in the previous section.

Transient Properties

Between the different rheological tests, the transient experiments are known to be a very good method to study the microstructure of complex fluids, such as polymer blends [69, 70]. The relative start-up shear stress of the neat components and their blends is shown in Fig. 9. The relative shear stress (τ_r) is obtained through this relation:

TABLE 4. FZM fitted parameters for blends and pure components.

Sample code	β_1	α	τ_0 (s)	G_0 (Pa)	G_e (Pa)
TPS	0.22	0.00	1.67	59,121	51,163
LDPE	0.97	0.61	2.28	12,030	335
LTC20	0.85	0.55	2.67	30,844	1,920
LTC35	0.89	0.59	3.64	29,442	5,086
LTC60	0.88	0.61	10.14	28,413	11,599
LTU60	0.93	0.62	19.84	20,276	0
LTC75	0.81	0.63	60.21	95,893	41,142

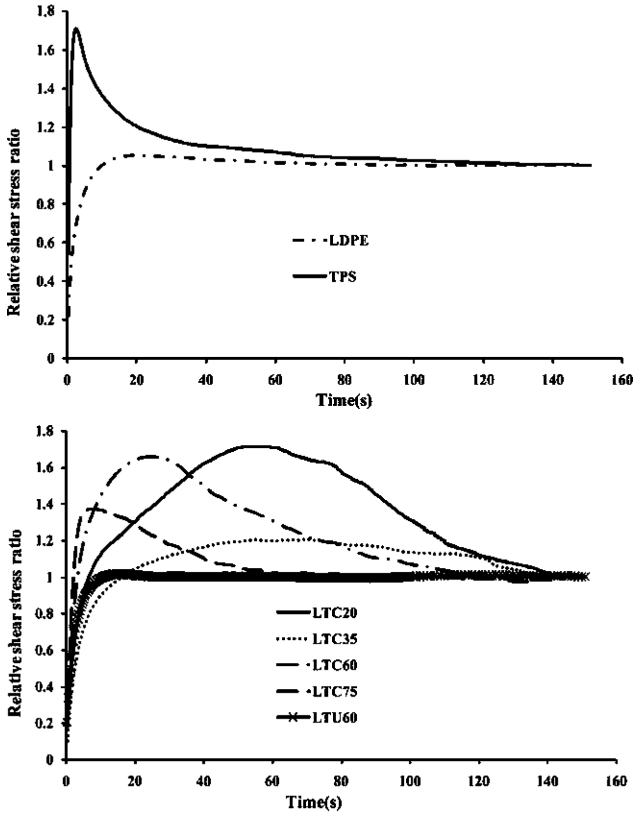

FIG. 9. The relative transient shear stress of (a) LDPE and TPS, and (b) LDPE/TPS blends.

$$\tau_r = \frac{\tau(t)}{\tau_{150}} \quad (12)$$

where $\tau(t)$ and τ_{150} are the shear stress at time t and 150 s (maximum time of the test). The transient shear stress of LDPE does not show any overshoot. Iza et al. reported similar results for pure HDPE and related this behavior to its shorter relaxation time [71]. On the other hand, TPS shows a strong overshoot at the beginning of the test that may originate from its elastic nature. Similarly, the compatibilized blends show strong overshoot. DeLeo et al. showed that the reactively compatibilized blends exhibited strong overshoot in the transient experiments and related this behavior to physical network, which comprised drop clusters [47].

At low TPS concentration, the overshoot time increased and broadened and the steady state was obtained very slowly. Edwards and Dressler showed that, with increasing capillary number, the stress overshoot broadened and higher strain units (longer times) should be applied to reach a steady-state value [72].

The capillary number is appropriate to the diameter of the droplet diameter and inversely appropriate to interfacial tension [73]. Because the diameters of the TPS particles of the samples are in the same range (Table 2), the difference in the interfacial tension leads to different capillary numbers. Therefore, the blends with lower TPS content, which show longer stress overshoot time, has lower interfacial tension. In other words, the compatibilizer is more effective at low TPS content.

Matos et al. showed that the apparent interfacial area, which is taken by a single compatibilizer molecule, is appropriate to the volume fraction of the dispersed phase and inversely appropriate to that of the compatibilizer [74]. Because the compatibilizer content is constant for all compatibilized blends (Table 1), the density of the compatibilizer at the interface (the number of compatibilizer molecules per unit area of interface) and therefore the interfacial tension decrease as the TPS content increases.

The transient shear stress of the uncompatibilized blend does not show any overshoot and reaches its steady state rapidly (shorter relaxation times). Entezam et al. showed that the uncompatibilized blends required shorter times than the compatibilized blends to reach their steady-state shear stress [30]. Therefore, it can be concluded that the short relaxation time of this blend was related to its poor compatibility because of the absence of the compatibilizer.

CONCLUSION

The morphological and rheological properties of the LDPE/TPS blends with and without compatibilizer at different component compositions were studied. The SEM images show that TPS does not tend to form co-continuous morphology except at very high concentration. Compatibilizer can decrease the diameter of the TPS phase significantly. In addition, the circularity ratio of the compatibilized blend is somewhat lower than the uncompatibilized blend. The blends show a pseudo-plastic behavior similar to the LDPE component. The elasticity and viscosity of the compatibilized blends are very much higher than the uncompatibilized blend, which implies the existence of TPS droplet clustering. The relaxation time peaks of the components shift toward longer times in the presence of the compatibilizer, which implies good compatibility between the two phases. The FZM model results proved the existence of a very elastic network in the compatibilized blends. The transient properties of compatibilized blends showed strong overshoots and long relaxation times that resulted from the formation of a high elastic network.

REFERENCES

1. M. Van der Burgt, M. Van der Woude, and L. Janssen, *J. Vinyl Addit. Technol.*, **2**, 170 (2004).
2. L. Janssen and L. Moscicki, Chapter 1: Biodegradable polymers and their practical utility, in *Thermoplastic Starch: A Green Material for Various Industries*, John Wiley & Sons, New York, 1 (2009).
3. L. Levitt and C.W. Macosko, *Macromolecules*, **32**, 6270 (1999).
4. M. Kaseem, K. Hamad, and F. Deri, *J. Polym. Sci. A*, **54**, 165 (2012).
5. X. Zhou, Y.Z. Liu, S.Y. Zhang, G.X. Zhang, and J.K. Wang, *J. Funct. Polym.*, **24**, 427 (2011).
6. W. Ning, Y. Jiugao, M. Xiaofei, and H. Chunmei, *Polym. Compos.*, **28**, 89 (2007).
7. A. Kahar, H. Ismail, and N. Othman, *J. Vinyl Addit. Technol.*, **18**, 65 (2012).

8. A. Wahab, M. Kahar, H. Ismail, and N. Othman, *J. Vinyl Addit. Technol.*, **18**, 192 (2012).
9. R. Sailaja, A.P. Reddy, and M. Chanda, *Polym. Int.*, **50**, 1352 (2001).
10. R. Sailaja, *Polym. Int.*, **54**, 286 (2005).
11. D. Bikiaris, J. Prinos, and C. Panayiotou, *Polym. Degrad. Stab.*, **56**, 1 (1997).
12. D. Bikiaris, J. Prinos, C. Perrier, and C. Panayiotou, *Polym. Degrad. Stab.*, **57**, 313 (1997).
13. D. Bikiaris, J. Prinos, and C. Panayiotou, *Polym. Degrad. Stab.*, **58**, 215 (1997).
14. R. Sailaja and M. Chanda, *J. Appl. Polym. Sci.*, **86**, 3126 (2002).
15. D. Bikiaris and C. Panayiotou, *J. Appl. Polym. Sci.*, **70**, 1503 (1998).
16. R. Sailaja and M. Chanda, *J. Polym. Mater.*, **17**, 165 (2000).
17. W. Liu, Y. J. Wang, and Z. Sun, *J. Appl. Polym. Sci.*, **88**, 2904 (2003).
18. Y. J. Wang, W. Liu, and Z. Sun, *J. Appl. Polym. Sci.*, **92**, 344 (2004).
19. M. Sabetzadeh, R. Bagheri, and M. Masoomi, *J. Appl. Polym. Sci.*, **126**, 63 (2012).
20. S. Wang and J. Yu, *Polym. Int.*, **54**, 279 (2005).
21. D. Ramkumar, M. Bhattacharya, and U.R. Vaidya, *Eur. Polym. J.*, **33**, 729 (1997).
22. J.C. Lepers, B.D. Favis, and R.J. Tabar, *J. Polym. Sci., Part B: Polym. Phys.*, **35**, 2271 (1997).
23. H. Liang, B. Favis, Y. Yu, and A. Eisenberg, *Macromolecules*, **32**, 1637 (1999).
24. J. Lyngaae-Jorgensen, L. D. Thomsen, K. Rasmussen, K. Sondergaard, and F. Andersen, *Int. Polym. Process.*, **2**, 123 (1988).
25. Y. Germain, B. Ernst, O. Genelot, and L. Dhamani, *J. Rheol.*, **38**, 681 (1994).
26. F. C. Chang and Y. C. Hwu, *Polym. Eng. Sci.*, **31**, 1509 (1991).
27. L. Utracki and P. Sammut, *Polym. Eng. Sci.*, **28**, 1405 (2004).
28. S. Velankar, P. Van Puyvelde, J. Mewis, and P. Moldenaers, *J. Rheol.*, **48**, 725 (2004).
29. C. Sailer and U. Handge, *Macromolecules*, **40**, 2019 (2007).
30. M. Entezam, H.A. Khonakdar, A.A. Yousefi, S.H. Jafari, U. Wagenknecht, G. Heinrich, and B. Kretzschmar, *Macromol. Mater. Eng.*, **297**, 312 (2011).
31. W. Ning, Y. Jiugao, M. Xiaofei, and W. Ying, *Carbohydr. Polym.*, **67**, 446 (2007).
32. Y. Jiugao, W. Ning, and M. Xiaofei, *Starch/Staerke*, **57**, 494 (2005).
33. G. Li and B.D. Favis, *Macromol. Chem. Phys.*, **211**, 321 (2010).
34. U. Sundararaj and C. Macosko, *Macromolecules*, **28**, 2647 (1995).
35. J. Li, P.L. Ma, and B.D. Favis, *Macromolecules*, **35**, 2005 (2002).
36. S.P. Lyu, T.D. Jones, F.S. Bates, and C.W. Macosko, *Macromolecules*, **35**, 7845 (2002).
37. W.E. Baker, C.E. Scott, and G.H. Hu, Chapter 5: Morphological and Rheological Aspects of Reactive Polymer Blending, in *Reactive Polymer Blending*, Hanser, Munich 109 (2001).
38. S. Steinmann, W. Gronski, and C. Friedrich, *Polymer*, **42**, 6619 (2001).
39. C. Weis, J. Leukel, K. Borkenstein, D. Maier, W. Gronski, C. Friedrich, and J. Honerkamp, *Polym. Bull.*, **40**, 235 (1998).
40. C. DeLeo, K. Walsh, and S. Velankar, *J. Rheol.*, **55**, 713 (2011).
41. B. Conde-Petit and F. Escher, *J. Rheol.*, **39**, 1497 (1995).
42. G. Della Valle, A. Buleon, P. Carreau, P.A. Lavoie, and B. Vergnes, *J. Rheol.*, **42**, 507 (1998).
43. F. Rodriguez-Gonzalez, B. Ramsay, and B. Favis, *Carbohydr. Polym.*, **58**, 139 (2004).
44. J.C. Scanlan and H.H. Winter, *Macromolecules*, **24**, 47 (1991).
45. H. Richtering, K. Gagnon, R. Lenz, R. Fuller, and H. Winter, *Macromolecules*, **25**, 2429 (1992).
46. A. Izuka, H.H. Winter, and T. Hashimoto, *Macromolecules*, **25**, 2422 (1992).
47. C.L. DeLeo and S.S. Velankar, *J. Rheol.*, **52**, 1385 (2008).
48. L. Bélard, P. Dole, and L. Avérous, *Polym. Eng. Sci.*, **49**, 1177 (2009).
49. L. A. Utracki, Chapter 7: The rheology of polymer alloys and blends, in *Polymer Blends Handbook*, Kluwer Academic Publishers, London, 449 (2002).
50. W. Wang, Y. Cao, J. Wang, and Q. Zheng, *J. Appl. Polym. Sci.*, **112**, 953 (2009).
51. I. Aravind, K.H. Ahn, C. Ranganathaiah, and S. Thomas, *Industr. Eng. Chem. Res.*, **48**, 9942 (2009).
52. S. Bose, M. Mukherjee, T. Rath, C. Das, and A. Saxena, *J. Reinf. Plast. Compos.*, **28**, 157 (2009).
53. B. John, K. Varughese, Z. Oommen, and S. Thomas, *Polym. Eng. Sci.*, **50**, 665 (2010).
54. D. Paul and J. Barlow, *J. Macromol. Sci. Rev. Macromol. Chem.*, **18**, 109 (1980).
55. Y. Fang, P.J. Carreau, and P.G. Lafleur, *Polym. Eng. Sci.*, **45**, 1254 (2005).
56. C. Lacroix, M. Aressy, and P.J. Carreau, *Rheol. Acta*, **36**, 416 (1997).
57. J.D. Ferry, Chapter 4: Approximate interrelations among the linear viscoelastic functions, in *Viscoelastic Properties of Polymers*, Wiley, New York, 80 (1980).
58. T.J. McCallum, M. Kontopoulou, C.B. Park, E.B. Muliawan, and S.G. Hatzikiriakos, *Polym. Eng. Sci.*, **47**, 1133 (2007).
59. M. Moan, J. Huitric, P. Mederic, and J. Jarrin, *J. Rheol.*, **44**, 1227 (2000).
60. E. Van Hemelrijck, P. Van Puyvelde, S. Velankar, C.W. Macosko, and P. Moldenaers, *J. Rheol.*, **48**, 143 (2004).
61. C. Lacroix, M. Grmela, and P. Carreau, *J. Rheol.*, **42**, 41 (1998).
62. F. Mighri, M. Huneault, A. Ajji, G. Ko, and F. Watanabe, *J. Appl. Polym. Sci.*, **82**, 2113 (2001).
63. R.B. Bird, and O. Hassager, Chapter 4: The Generalized Newtonian Fluid, in *Dynamics of Polymeric Liquids: Fluid Mechanics*, Wiley, New York, 169 (1987).
64. F. Xie, P.J. Halley, and L. Avérous, *Prog. Polym. Sci.*, **37**, 595 (2012).
65. J. Palierne, *Rheol. Acta*, **29**, 204 (1990).
66. C. Sailer and U. Handge, *Macromolecules*, **41**, 4258 (2008).
67. W. Yu, W. Zhou, and C. Zhou, *Polymer*, **51**, 2091 (2010).
68. C. Friedrich, *J. Non-Newton Fluid.*, **46**, 307 (1993).
69. M. Iza and M. Bousmina, *J. Rheol.*, **44**, 1363 (2000).
70. M. Bousmina, M. Aouina, B. Chaudhry, R. Guénette, and R.E.S. Bretas, *Rheol. Acta*, **40**, 538 (2001).
71. M. Iza, M. Bousmina, and R. Jérôme, *Rheol. Acta*, **40**, 10 (2001).
72. B.J. Edwards and M. Dressler, *Rheol. Acta*, **42**, 326 (2003).
73. R.G. Larson, Chapter 9: Foams, emulsions and blends, in *The Structure and Rheology of Complex Fluids*, Oxford University Press, New York, 388 (1998).
74. M. Matos, B. Favis, and P. Lomellini, *Polymer*, **36**, 3899 (1995).